New condensed matter probes for diamond anvil cell technology

New condensed matter probes for diamond anvil cell technology

Viktor V Struzhkin, Russell J Hemley and Ho-kwang Mao

Geophysical Laboratory, Carnegie Institution of Washington, 5251 Broad Branch Road, NW, Washington, DC 20015, USA

Abstract

An overview of several new developments in diamond anvil cell techniques is presented. The novel techniques developed in our laboratory address fundamental properties of compressed materials, e.g. vibrational, electronic and spin excitations. We focus on the techniques made possible by third-generation synchrotron x-ray sources and by the development of the magnetic susceptibility probes in diamond anvil cells. A brief list of topics is given below:

(i) Application of nuclear resonant inelastic x-ray scattering technique to the measurements of the phonon density of states and elastic properties of iron-containing materials at megabar pressures.

(ii) Magnetic collapse and high-spin to low-spin transitions probed by the x-ray $K\beta$ emission process in transition metal compounds.

(iii) Superconductivity in multi-megabar pressure range studied by the magnetic susceptibility technique.

Selected applications of these techniques will be covered, including elastic properties of compressed hcp-Fe, insulator–metal transition in FeO and superconductivity in Li.

(Some figures in this article are in colour only in the electronic version)

1. Introduction

Diamond anvil cell (DAC) technology has developed rapidly during the past few years [1, 2]. A number of techniques that were previously limited to ambient pressure (because of the requirement of a large sample volume), may now be used at high and even ultrahigh pressures [3–11]. We will review recent developments at synchrotron facilities in phonon and electron spectroscopies, and also the progress in superconductivity studies at very high pressures close to the limit of current diamond anvil cells.
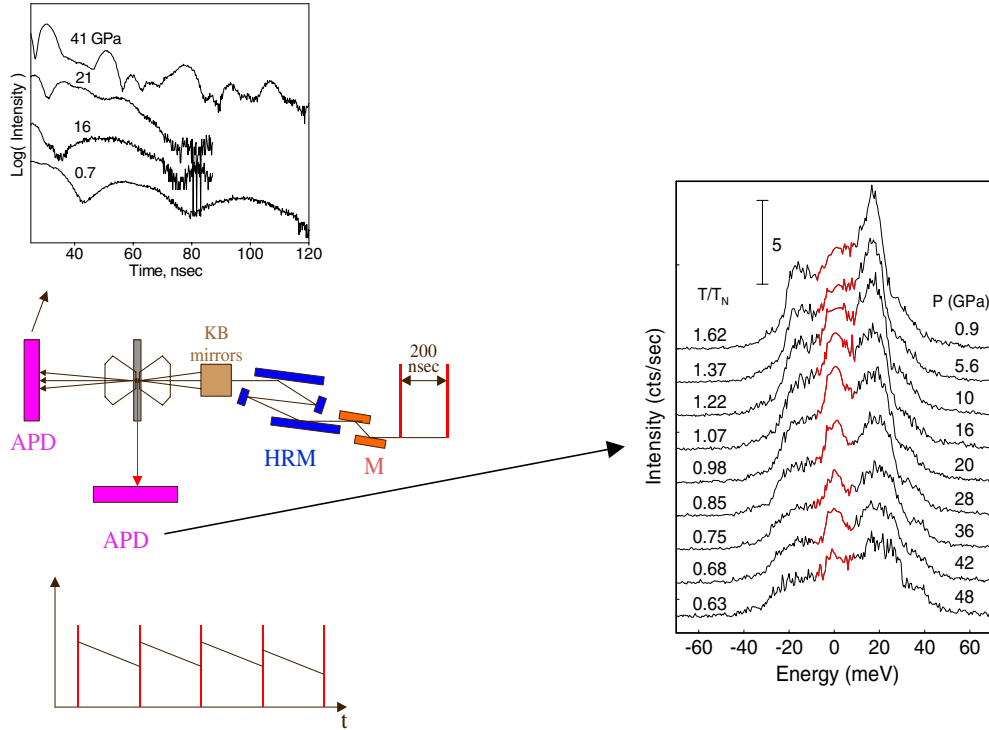
2. Nuclear resonant inelastic x-ray scattering technique at high pressures

The recent combination of high pressure methods and the nuclear resonant inelastic x-ray scattering (NRIXS) technique has produced important breakthroughs in understanding the elastic properties of iron and iron-containing materials at very high pressures up to 150 GPa [5]. This powerful combination is, at the moment, the only technique that can probe shear sound velocities in solids in the megabar pressure range. The nuclear resonant inelastic scattering technique is a relatively new method developed for measurements of phonon density of states (DOS) of samples containing Mössbauer-active isotopes. The method has been applied to a number of samples containing ^{57}Fe [12, 13]. The technique is particularly suitable for pure iron [4, 5]. Experiments at ambient conditions [14, 15] have already shown that NRIXS provides a very precise representation of the true DOS by direct comparison with neutron scattering [5] for body-centred cubic (bcc) Fe. Further high-pressure NRIXS measurements to 42 GPa [4] and 150 GPa [5] have demonstrated that the technique can be successfully applied for studies of materials at extremely high pressures, matching those of the Earth's outer core, and providing important information on aggregate average sound velocity, vibrational kinetic, energy, zero-point energy, vibrational heat capacity, Debye temperature, etc. Combined with compressibility measurements, these data can be used to extract longitudinal and shear sound wave velocities, important for the interpretation of the available seismic data of the Earth [5].

Mössbauer spectroscopy is typically performed in bench-top experiments using a radioactive source. There have been major advances that exploit the temporal structure of synchrotron radiation to perform nuclear resonance spectroscopy (Mössbauer spectroscopy) in the time domain [16]. In this application, highly monochromatized x-rays from the synchrotron are used to excite narrow nuclear resonances and the delayed photons are detected. Hyperfine splitting can then be reconstructed from the time-dependent intensity. In addition, the phonon density of states for the vibrations of Mössbauer-active nuclei can also be measured [12]. We present below a brief description of this experimental technique in its application to high-pressure studies. Our experiments were performed at the synchrotron beamline SRI-CAT 3ID of the Advanced Photon Source (APS), Argonne National Laboratory. The high resolution (2 meV) monochromator scans in the range 100 meV (referencing the 14.4125 keV nuclear transition of ^{57}Fe) with 0.4 meV steps were used to collect the data. An incident ($600 \times 200~\mu m^2$) monochromatic x-ray beam was collected by two orthogonal Kirkpatrick–Baez (KB) mirrors [17] and focused to less than $10 \times 10~\mu m^2$ on the sample in a diamond anvil cell (figure 1). The direct beam passing through the sample and both diamond anvils is recorded by an avalanche photodiode detector (APD) for Mössbauer measurements in the time domain (nuclear resonant forward scattering) and as the zero-energy reference marker. The elastic and inelastic resonant excitation can be observed by the detection of x-ray fluorescence (Ka and Kb) resulting from subsequent nuclear deexcitation. The inelastic signal is collected by three APDs mounted as close to the sample as possible; the details of the diamond anvil cell design are reported elsewhere [5]. The Fe and FeO samples were about 25 μm in diameter (loaded with a He pressure medium) and the diamonds with flat 400 μm formers were used. The measured spectra, i.e. count rate as a function of the energy difference between the incident photon energy and the nuclear transition energy, were converted to phonon DOS according to the data analysis procedure described by Hu *et al* [14]. Typically 10–20 DOS spectra (1 h / spectrum) at the same pressure were summed. Pressure was measured using the ruby R_1 fluorescence line and the pressure scale from [18].

2.1. Iron

Iron transforms under pressure from the bcc to the hcp phase between 13 and 20 GPa. The transformation range depends on the pressure medium used; substantial hysteresis (5 GPa) is

Figure 1. Nuclear inelastic resonant x-ray scattering set-up for measurements in the diamond anvil cell. The viewgraphs illustrate the pressure evolution of the nuclear forward scattering spectra of FeO (top) and nuclear resonant inelastic x-ray scattering spectra of FeO (right) through the pressure-driven transition from the paramagnetic (NaCl structure) to the antiferromagnetic (rhombohedral structure) phase above 17 GPa.

observed even with the most hydrostatic solid pressure medium (helium). We have measured NRIXS in pure Fe both in nonhydrostatic [5] and nearly hydrostatic conditions (He pressure medium). Below we will discuss the high-pressure hcp phase of Fe. Previous nonhydrostatic results to 150 GPa were used to deduce longitudinal and shear sound wave velocities [5]. The analysis presented in [5] depends on the assumption that longitudinal and shear aggregate sound velocities can be used to calculate the Debye sound velocity. We present below the outline and limitations of these calculations and compare the nonhydrostatic with the nearly hydrostatic results. As was shown previously [4, 5], the density of the phonon states in the low-frequency region can be used to calculate average Debye sound velocity, which can be written in the form [5]

$$3V_{\mathrm{D}}^{-3} = V_{\mathrm{P}}^{-3} + 2V_{\mathrm{S}}^{-3} \tag{1}$$

where V_{D}, V_{P} and V_{S} are the Debye, longitudinal, and shear sound velocities, respectively. V_{P}^{-3} and V_{S}^{-3} should be taken as values averaged over all directions in the case of anisotropic sound velocities, and $2V_{\mathrm{S}}^{-3} = V_{\mathrm{S1}}^{-3} + V_{\mathrm{S2}}^{-3}$, where V_{S1}^{-3} and V_{S2}^{-3} are orientational average values for quasi-compressional and pure shear wave branches. The expressions for $V_{\mathrm{P}}(Q)$, $V_{\mathrm{S1}}(Q)$ and $V_{\mathrm{S2}}(Q)$ in terms of the elastic constants C_{ij} and the angle Q between the phonon k-vector and the G–A direction for the hcp crystal can be found in [19]. We rewrite these expressions below and give the anisotropic contributions explicitly:

$$rV_{\mathrm{P}}^2 = (A + B)/2 \tag{2a}$$

$$r V_{S1}^2 = C_{44} + (1/2)(C_{11} - C_{12} - 2C_{44}) \sin^2(Q) \tag{2b}$$

$$r V_{S2}^2 = (A - B)/2 \tag{2c}$$

$$A = C_{11} + C_{44} + (C_{33} - C_{11}) \cos 2(Q) \tag{2d}$$

$$B = (1/2)\{(C_{11} - C_{33})^2 + 4(C_{13} + C_{44})^2 - 2(C_{11} - C_{33})(C_{11} + C_{33} - 2C_{44}) \cos(2Q)$$
$$+ [(C_{11} + C_{33} - 2C_{44})^2 - 4(C_{13} + C_{44})^2)] \cos^2(2Q)\}^{1/2} \tag{2e}$$

where r is the density of the material. From equation (2b) the condition for the isotropic quasicompressional sound velocity V_{S1} is given by

$$C_{66} = (1/2)(C_{11} - C_{12}) = C_{44} \tag{3}$$

while, according to equations (2a), (2c)–(2e), the isotropy of longitudinal and pure shear waves would require two conditions to be met:

$$C_{11} = C_{33}, \tag{4a}$$

$$C_{11} + C_{33} - 2C_{44} = 2(C_{13} + C_{44}). \tag{4b}$$

Equations (3) and (4) are sufficient to deduce all five elastic constants for the isotropic hcp crystal from two independent constants C_{11} and C_{44}. The remaining tree elastic constants are $C_{33} = C_{11}, C_{12} = C_{13} = C_{11} - 2C_{44}$. For the isotropic case, when equations (3) and (4) are valid, there is no dependence on the angle Q and the averaged velocities can be substituted by the isotropic values expressed in terms of two independent elastic constants C_{11} and C_{44}:

$$r V_P^2 = C_{11}, \qquad r V_S^2 = C_{44}. \tag{5}$$

In [5] two additional conditions are considered:

$$K/r = V_P^2 - (4/3)V_S^2 \tag{6}$$

$$G/r = V_S^2 \tag{7}$$

where K and G are bulk and shear modulus, respectively, and V_P and V_S are average isotropic longitudinal and shear sound velocities. Here, however, the averaging procedure differs from the averaging scheme presented above for the Debye sound velocity. Different averaging schemes exist for polycrystals: the most commonly used is the Voigt–Reuss average, which is an ad hoc arithmetic average between Voigt and Reuss values. More precise Hashin–Shtrikman bounds [20] are used quite often, which can be written explicitly for the hcp crystal [21]. The Voigt and Reuss expressions for the bulk modulus K [21] are usually very close to each other and can be used as an estimate of the adiabatic bulk modulus K. However, the Voigt and Reuss expressions for the shear modulus G differ significantly in the case of substantial anisotropy in sound wave velocities [21, 22]. The resulting estimate for the shear sound wave velocity from equation (7) will vary depending on the approximation used. It can be shown (at least for the hcp crystal) that for the isotropic solid sound wave velocities determined from different expressions for the shear modulus (Voigt, Reuss and Hashin–Shtrikman bounds [21]) merge into a single expression given by equation (7), with V_S given by equation (5). Similarly, equation (6) also becomes exact in the isotropic case, with V_P given by equation (5). However, in the anisotropic case the averaging procedure depends critically on the approximation used for the determination of the shear modulus G. Thus, the anisotropic case requires more elaborate analysis; the expressions given by equation (1), and equations (6) and (7), contain different averages and cannot be used as a closed set of equations in contrast to the isotropic case. An example of the anisotropic dependence of the sound wave velocities of hcp-Fe at 50 GPa is shown in figure 2, as derived from radial diffraction measurements [24]. The corresponding average values of the sound wave velocities are also shown. There is a substantial difference between different average values, depending on the averaging procedure used. The value for the longitudinal
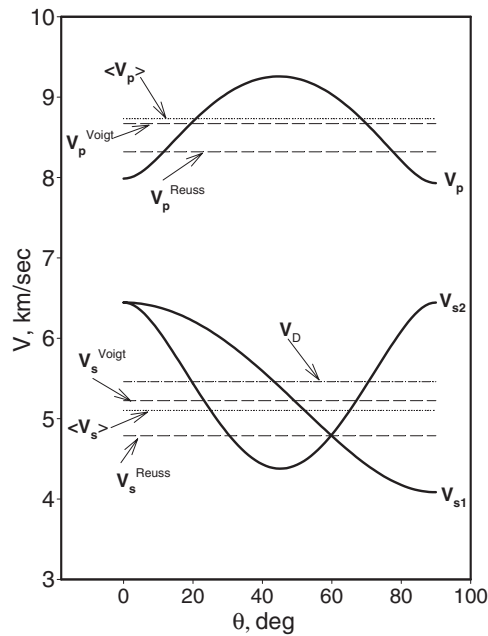
Figure 2. Anisotropy of sound velocities in hcp-Fe at 50 GPa. The elastic constants (in GPa) $C_{11} = 639$, $C_{33} = 648$, $C_{12} = 300$, $C_{13} = 254$, $C_{44} = 422$ and $\rho = 10.16$ g cm^{-3} from [24] were used. The Voigt and Reuss average values were calculated using equations (6) and (7), while the corresponding K and G values were estimated using standard expressions from [21]. Average values (dotted lines) were calculated as orientational averages.

sound wave averaged over all directions Q is calculated to be $V_P = 8.73$ km s^{-1}, which can be compared with the measured value $V_P = 8.03 \pm 0.23$ km s^{-1} at 55 GPa from inelastic x-ray scattering experiments on hcp-Fe without a pressure medium [23]. The value calculated from radial diffraction data is higher, but the discrepancy may be well within the experimental error of both techniques. On the other hand, substantial elastic anisotropy [24] and preferred orientation effects [25] may be responsible for the observed difference. The Debye average velocity calculated from the radial diffraction data [24] is $V_D = 5.46$ km s^{-1}, which is also higher than the experimental value 5.0 ± 0.25 km s^{-1} determined by the NRIXS technique [5]. Notably, recent nearly hydrostatic measurements in a He pressure medium [26] give even lower $V_D = 4.53$ km s^{-1} at 50 GPa. This variation in experimental values is comparable to the spread in average $V_S^{\text{Voigt,Reuss}}$ values shown in figure 2; it may indicate a substantial elastic anisotropy of hcp-Fe. Further experiments probing the anisotropy in the inelastic x-ray scattering [27] are required to establish the anisotropy of the elastic properties of hcp-Fe, which can be used in the interpretation of the anisotropy in the geophysical seismic data. Furthermore, experimental results of inelastic scattering experiments [5, 23] are extrapolated to the pressures at the Earth's core. It is apparent from the previous discussion that these extrapolations depend crucially on the extent of the preferred orientation [24] and elastic anisotropy of hcp-Fe.

2.2. Iron oxide

The study of the electronic and magnetic properties of simple transition metal compounds is an important topic in diverse fields, ranging from solid-state physics to Earth sciences. Iron oxide (FeO) belongs to the group of highly correlated transition metal oxides, being an
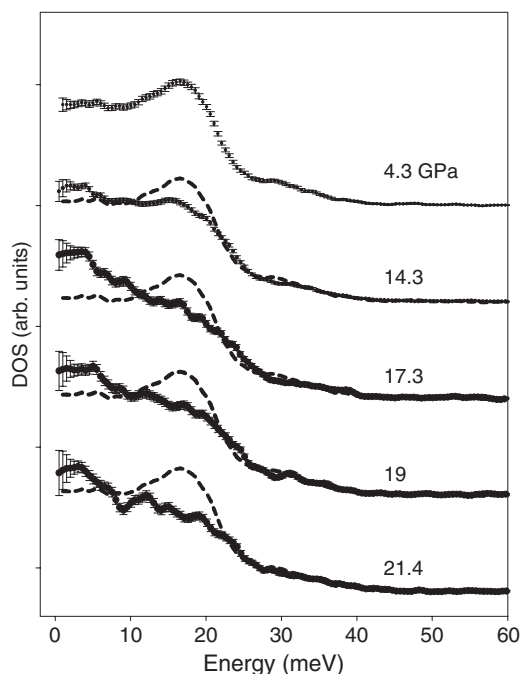
Figure 3. We show $g(E)/E^2$ calculated from the density of states $g(E)$ in FeO in a He pressure medium at several pressures. The 4.3 GPa data are shown as a broken curve for comparison with higher pressure data. The low-energy anomaly is most pronounced at 17.3 GPa, close to the pressure-induced transition to the antiferromagnetic Néel state.

archetypal insulating antiferromagnetic material at zero temperature. FeO stands out from this group of materials, because it is a possible major constituent of the Earth's lower mantle and upper core; thus, its pressure- and temperature-dependent properties are very important for our understanding of the Earth's interior. Our recent studies of the vibrational density of states of ^{57}Fe-isotope-enriched $Fe_{0.95}O$ by high-resolution nuclear resonance inelastic x-ray scattering have been reported in [28]. The apparent feature of the experimental results in figures 1 and 3 is an inelastic peak at small energy transfers. It is most pronounced near 16 and 20 GPa in nonhydrostatic measurements (figure 1), and at 17.3 GPa in nearly hydrostatic measurements (figure 3). This is exactly the pressure range of the reported transition from the paramagnetic rock-salt-type structure to the antiferromagnetic rhombohedral structure [29, 30]. The transition is very sensitive to the nonhydrostatic stress [29]; for example, the splitting of the (111) diffraction line is smeared between 10 and 18 GPa without a pressure medium and occurs around 16 GPa [29] to 17 GPa [31] under nearly hydrostatic conditions.

We thus observe a pronounced softening of the low energy vibrational spectrum close to the pressure-induced Néel transition. The resolution of the present measurements (2 meV) does not allow us to follow the softening to the low-frequency region, where most static and ultrasonic measurements are performed. However, this behaviour suggests large effects on the static elastic constants at the Néel transition. The calculated dispersion relations for FeO at 28 GPa modified by magnetoelastic coupling are shown in figure 4 (estimated at $T = 295$ K); the corresponding sound velocities are also shown. Dispersion relations—figure 4(b)—for the coupled branches change by less than 1 meV compared to the bare (uncoupled) branches, well within the resolution of the neutron inelastic scattering experiment. However, as is evident from figure 4(b), the effect on the sound velocities is more pronounced, being almost 20–30%
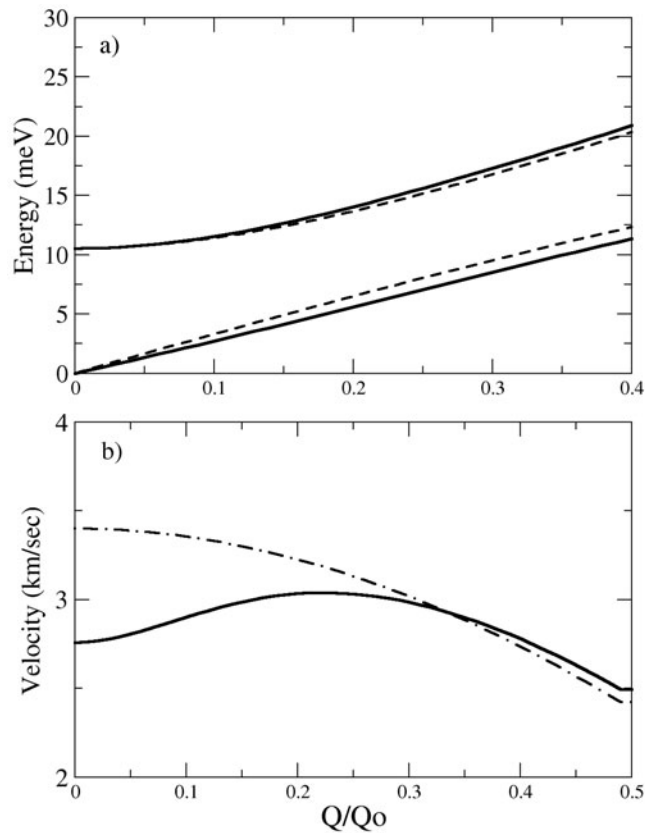
Figure 4. Model for the magnetoelastic coupling in FeO [28]. (a) The interacting transverse phonon and magnon branches. Noninteracting bare frequencies are shown by broken lines, the dispersion branch for magnons is calculated according to [28] and the phonon dispersion was approximated by $E(Q) = 2Q_0(V_s/\pi)\sin(\pi/2(Q/Q_0))$ using the sound velocity $V_S = 3.4 \text{ km s}^{-1}$ at $Q = 0$. (b) Calculated sound velocity including magnetoelastic coupling (full curve) and without magnetoelastic coupling (chain curve).

within the energy transfer range up to 5 meV. This agrees reasonably well with the enhancement of the density of states that we observe in our experiment (figure 3). At present we do not have enough experimental information and theoretical understanding to better constrain the magnetoelastic coupling at $T-T_N$. As follows from our observations however, the effect is most pronounced close to the Néel transition. Close to $T-T_N$ the classical description given in [28] is no longer valid and spin fluctuation effects should be included appropriately [32]. Our observations support the Mössbauer measurements, where the magnetic transition was observed starting from 8 GPa under nonhydrostatic conditions. The reason for that is the uniaxial strain developing along the body diagonal which may induce magnetic moments well below the transition point determined under hydrostatic conditions (17 GPa). This is consistent with the notion that this second-order phase transition is smeared by the external field (uniaxial strain), which is proportional to the order parameter of the broken symmetry phase [33].

3. Kβ emission process as spin state indicator in transition metal compounds

The Kβ x-ray emission has been used for several decades at ambient conditions to study the spin state and the valence state of transition metal ions. Recently we have applied this
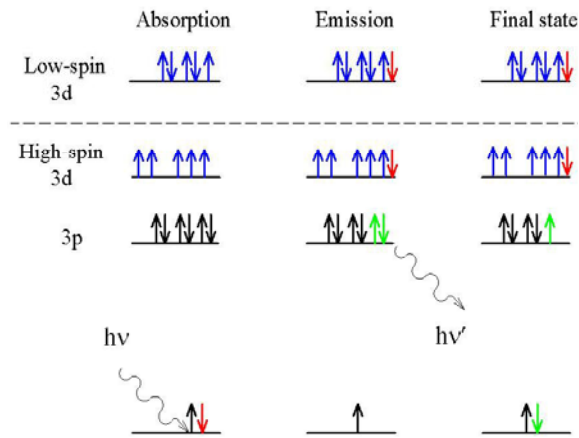
Figure 5. The schematic diagram of the Kβ emission process.

technique to compressed materials. The pressure-induced high-spin to low-spin transition has been observed in FeS [34]. A similar study on FeO [35] has provided a probe of the spin state of Fe^{2+} to 140 GPa (close to pressure conditions at the Earth's core–mantle boundary). We present below an outline of the set-up used in these studies and briefly describe recent results.

3.1. Technique

The process of Kβ emission is illustrated in figure 5. The emission results from the 3p $\rightarrow$ 1s decay. The Kβ lineshape can be described, to a good approximation, using a two-step model (absorption followed by emission). In the final state a 3p core hole strongly interacts with the incomplete 3d shell. The consequence is the splitting of the Kβ spectrum into two peaks, whose separation is controlled by the configuration interaction in the final state. The splitting usually exceeds the 3p–3d simple exchange interaction J. Furthermore, the calculations show that the Kβ' satellite at lower energy results predominantly from the 3p $\uparrow$ 3d $\uparrow$ final state whereas the K$\beta^{1,3}$ line comes mainly from a 3p $\uparrow$ 3d $\downarrow$ final state with a small contribution of the 3p $\uparrow$ 3d $\uparrow$, which appears in the spectrum as a low energy shoulder in the main peak.

Below is a short list of the components for the high pressure XES experiment:

- upstream collimating and focusing optics (we used focusing KB mirrors [17], providing an x-ray spot less than 10 μm in diameter);
- Rowland-circle spectrometer including the Si or Ge crystal analyser and the detector. The x-ray beam path should be filled with He gas or placed in a vacuum to minimize signal losses and background radiation due to x-ray scattering in air [34];
- high-pressure cell with a beryllium gasket to allow measurements of the x-ray emission at low energy [34].

High-energy third-generation synchrotron sources provide an intense x-ray beam. However, the x-ray emission may be completely absorbed by the traditional stainless steel gaskets and severely attenuated in diamond in the range of Kβ emission in 3d elements. We have used a Be gasket which is nearly transparent to x-rays at the K edge of Fe.

3.2. Selected results

Previous high-pressure experiments on Kβ emission have not addressed the pressure-induced shift of the Kβ line because of the strict requirements for the reproducibility in the sample
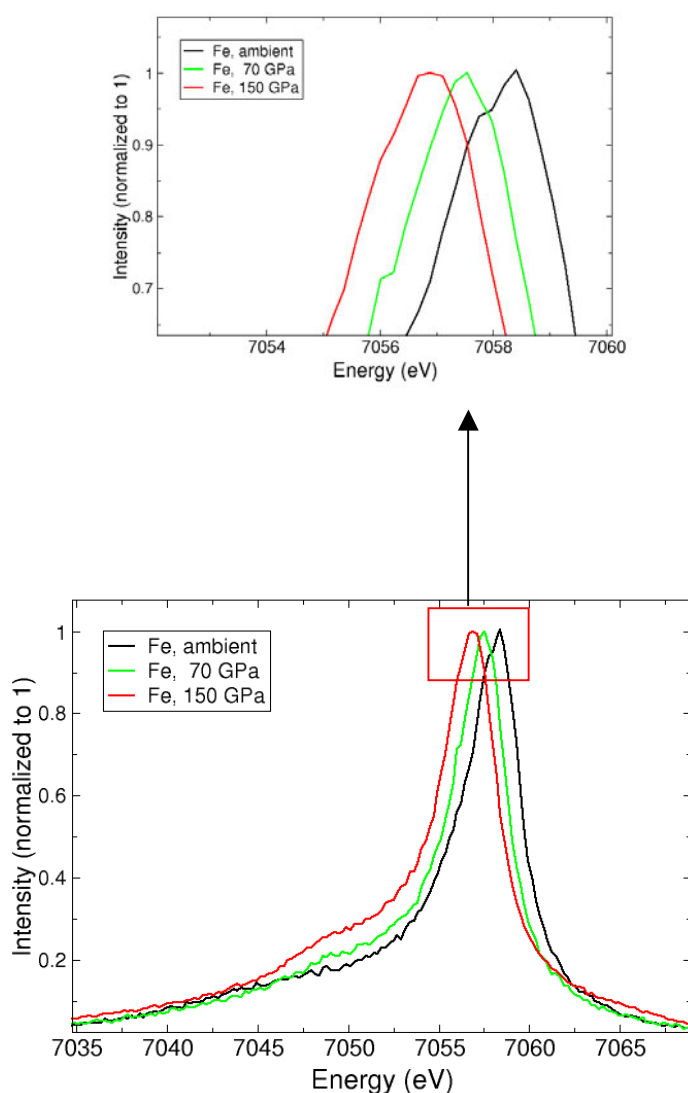
Figure 6. Kβ emission spectra of pure Fe to 150 GPa.

position [34–36]. Recently we have designed high pressure experiments which take advantage of the tight x-ray focus ($<$10 μm in diameter) after the KB mirrors. Reproducible sample positioning and small sample size (20–30 μm) allowed the measurements of the Kβ line position in iron with an accuracy of 0.15 eV (0.002%). The lineshift was about 1 eV/100 GPa— see figure 6.

We have used a set-up similar to that in [34], but with the Rowland-circle plane perpendicular to the incoming x-ray beam. In this configuration the detector is mounted above the sample, and the Be gasket is perpendicular to the x-ray beam. The tight x-ray focus provides a much better local probe of the sample than in the horizontal set-up [34]. The sample position is actually defined by the x-ray beam focus, which is extremely stable and well defined. In this arrangement the incoming x-ray beam is directed through the diamonds

and the intensity on the sample is attenuated by the absorption of one of the diamond anvils. The attenuation of the x-ray intensity at 12 keV is about a factor of 2 for the diamond height of 1.3 mm, increasing rapidly for larger diamonds. With this set-up we have recently measured the Kβ emission and x-ray diffraction of FeO and $Mg_{0.5}Fe_{0.5}O$ in the 100 GPa pressure range with and without pressure media, using laser heating to relieve the stresses in the compressed samples. We have observed the pressure-induced shift of the main Kβ emission peak, which was similar to the pure Fe. The observed changes in the Kβ emission suggest a metallic state at about 100 GPa [37]. Further studies of electrical and optical properties are underway to resolve the stability field of the low-spin and metallic states in FeO at high pressure conditions.

3.3. Discussion

Unambiguous identification of the high-spin to low-spin transition in insulating or semiconducting materials similar to FeS [34] is not straightforward in metals. For example, the high-spin satellite feature in pure iron is much lower (figure 7) compared to FeS, FeO or Fe_2O_3 [34, 35]. Despite these difficulties the transition to the low-spin state was observed in pure Fe between 13 and 20 GPa [36] from precise measurements of the Kβ emission lineshape. However, additional complications are involved when an insulator–metal transition accompanies the changes in the Kβ emission lineshape. Our experimental data [37] suggest that the metallic state is stabilized in FeO above 100 GPa. The corresponding x-ray emission spectra of FeO are shown in figure 7. The transition to the metallic state depends on the pressure medium used and is sensitive to the pressure distribution in the sample. We believe that the broadening of the d and p bands under pressure (figure 7) is responsible for the observed transition. The identification of the spin state of the Fe^{2+} ion at these conditions requires a better theoretical understanding of the electronic correlation effects, their coupling to the lattice degrees of freedom (magnetoelastic coupling effects) and an improved theoretical description of the Kβ emission process in the metallic state.

At low pressures, iron–oxygen alloys form immiscible melts consisting of iron-rich metallic and iron oxide non-metallic components. Thus, for oxygen to be an important alloying constituent of iron in the core, it must become miscible with liquid iron at high pressure. According to current understanding the more compact low-spin Fe^{2+} ion favours metallic bonding in FeO already at moderate temperatures above 100 GPa. The identification of the metallic low-spin state of iron in iron oxide may provide an explanation of the FeO miscibility with liquid Fe in the Earth's outer core.

4. Superconductivity at multi-megabar pressures: magnetic susceptibility technique

As a result of the rapid development of diamond-cell techniques, a broad range of studies of the physical and chemical properties of solids can now be conducted *in situ* at high pressures above 100 GPa. The application of pressure provides an ideal means to carefully tune electronic, magnetic, structural and vibrational properties for a wide range of applications [1, 2]. High pressures of about 30 GPa have been used to create one of the highest T_c superconductors known to date ($HgBa_2Ca_2Cu_3O_{8+\delta}$), with a critical superconducting temperature of 164 K [38]. The same material holds the record $T_c = 133$ K at ambient pressure. Notably, it was a consideration of the effect of pressure on the 40 K cuprates [39] that guided those experiments leading to the 91 K superconductor [40].

Earlier techniques have been adapted for very small sample volumes (a typical sample size in a high pressure experiment is about $100 \times 100 \times 20 \ \mu m^3$ at 30 GPa) to measure superconducting transitions inductively (by using magnetic susceptibility methods) at high
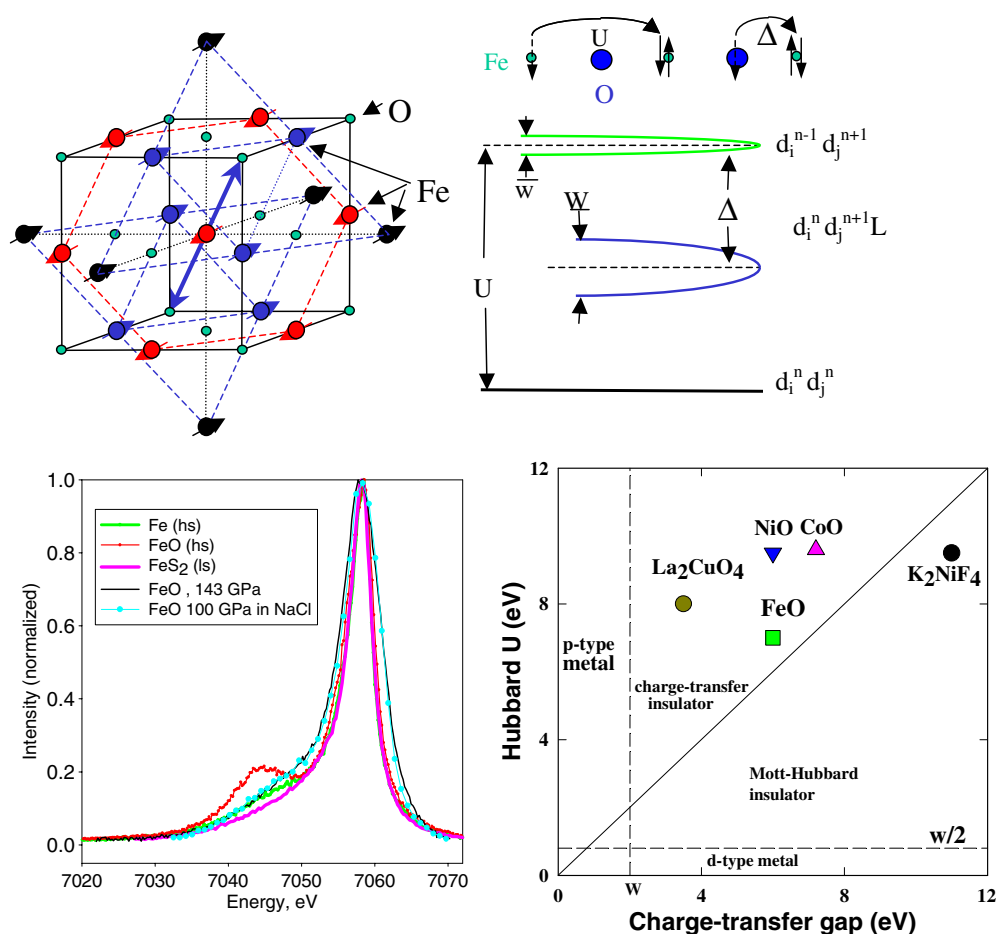
Figure 7. Top left: NaCl-type crystal structure of the FeO sample below 17 GPa at room temperature. The structure has a small rhombohedral distortion (elongation along a body diagonal) in the antiferromagnetic phase above 17 GPa. Top right: electronic states in the material. It is energetically unfavourable for the electron to move between Fe atoms. Such a transition costs an energy U (Hubbard energy). The transition of the electron from an oxygen atom to a neighbouring Fe atom is also energetically unfavourable; the energy cost for such a transition is called the charge-transfer energy Δ. Bottom right: Zaanen–Sawatzky–Allen diagram, illustrating the balance between Hubbard energy U and charge transfer energy Δ in several strongly correlated materials. Bottom left: x-ray emission spectra of high-spin FeO at ambient pressure, high-spin Fe at ambient pressure and metallic FeO at 100 GPa. Low-spin XES of FeS_2 are shown for comparison.

pressures. The samples must be further reduced in size when a pressure medium is used (which is mandatory for many applications), and also for very high pressure experiments, above 100 GPa. To handle these demanding tasks new methods have been invented and developed to measure superconducting transitions by magnetic techniques. We present here a discussion of a relatively new double-frequency modulation technique. The technique was used in recent measurements of T_c in sulfur to 230 GPa without a pressure medium [41] and in measurements of superconductivity in MgB_2 to 45 GPa in He pressure media [42]. Recent results for superconductivity in simple s–p metals will be presented, specifically superconductivity in compressed Li [43].

4.1. Overview of the technique

We give an overview here of recent progress in the development of magnetic susceptibility techniques for diamond-anvil cell applications. The method presented here was described in [44]. We have addressed the details of the measurements of superconducting critical temperatures by magnetic susceptibility recently [45, 46]. Here we will present an outline of the technique. We begin with a discussion of the problems that arise when measuring magnetic properties of a small superconducting sample in a system consisting of signal and compensating (secondary) and exciting (primary) inductance coils located in the vicinity of the sample (figure 8). The exciting coil (1) creates an alternating magnetic field which produces electromotive forces in both the signal (3) and compensating (2) coils. These coils are included in the electrical circuit in such a manner that their electromotive forces act in opposite directions and nearly compensate for each other. The difference between the two electromotive forces determines the background signal whose magnitude depends on several factors. The most significant are:

 (a) differences in the geometric parameters of the signal and compensating coils and their unavoidable asymmetric disposition inside the exciting coil, and
 (b) the proximity of the system of coils to metal parts of the high-pressure chamber (not shown in the figure), which distort the uniform distribution of magnetic flux passing through the signal and compensating coils due to geometric asymmetry and electrical conductivity.

A modulation technique can be applied to detect the superconducting critical temperature due to the fact that one can 'virtually' remove the superconducting sample from the high pressure cell by applying an external magnetic field that destroys the superconductivity in the sample. The technique is based on the fact that the magnetic susceptibility of superconducting materials depends on the external magnetic field enclosed in the volume of the sample. When the magnetic field is high enough to quench the superconductivity, the magnetic field penetrates into the sample volume (this happens at the critical magnetic field H_c). In contrast, the susceptibility of the metallic parts of the high-pressure cell (diamagnetic and paramagnetic) is essentially independent of the external field. Thus, the insertion of the high-pressure cell containing the sample in an external magnetic field exceeding the critical value changes the part of the signal produced by the sample, while the background remains practically constant. This fact allows the separation of the signal arising from the sample from that of the background. We apply the low-frequency ($f = 22$ Hz) magnetic field with an amplitude up to several dozen oersteds (coil (4), figure 9), which causes the destruction of the superconducting state near the superconducting transition. This in turn leads to a change in the magnetic susceptibility of the sample from -1 up to 0 twice in a given period and produces a modulation of the signal amplitude in the receiving coils at a frequency $2f$. The subsequently amplified signal from the lock-in amplifier is then recorded as a function of temperature on the computer. The critical superconducting temperature T_c is then identified as the point where the signal goes to zero due to the transition of the sample to the normal state [46].

4.2. Superconductivity in Li

Lithium is considered the simplest metal: it is the lightest of the alkali metals and, under normal pressure–temperature conditions, its properties are well described within a nearly-free-electron model. Recent studies show that under pressure, however, this simple picture changes radically [47, 48]. Theoretical predictions suggest that lithium may undergo several structural transitions, possibly leading to a 'paired-atom' phase with low symmetry and near-insulating properties [47]. Though this prediction is the antithesis of the intuitive expectation
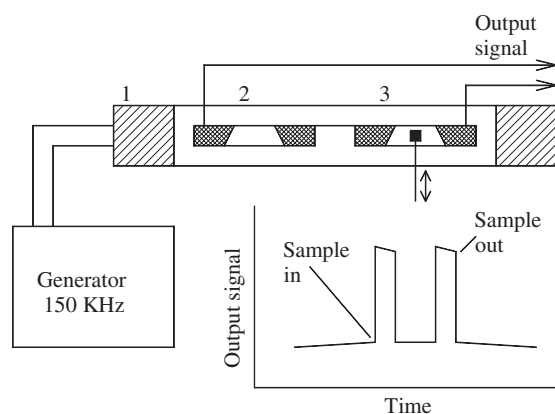
Figure 8. Schematic representation of the background subtraction principle in magnetic susceptibility measurements: 1—primary coil; 2—secondary compensating coil; 3—secondary signal coil. Removal of the sample from the signal coil produces measurable changes in the total output signal.
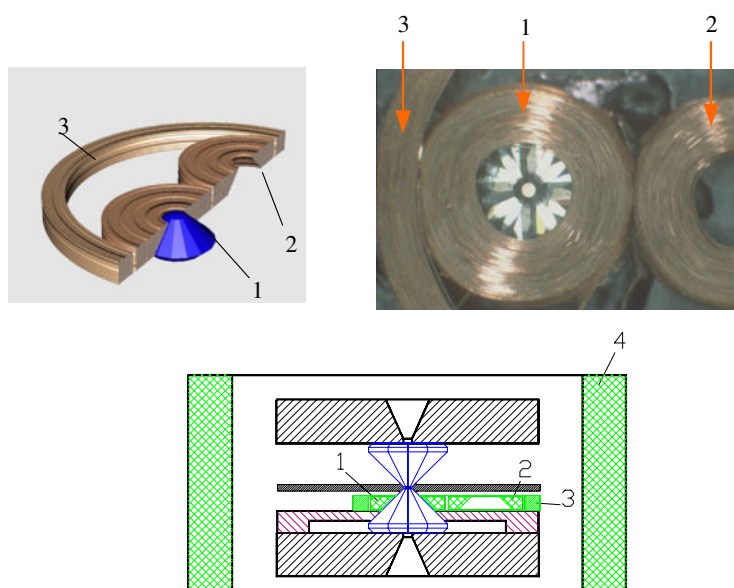

Figure 9. Double-frequency modulation set-up: coil 4 is used to apply a low frequency magnetic field to modulate the amplitude response from the high-frequency pick-up coil 2 due to the superconducting sample. The set-up includes two signal generators and two lock-in amplifiers, operating at low (20–40 Hz) and high (155 kHz) frequencies.

that pressure favors high-symmetry crystal structures with metallic properties, recent x-ray diffraction studies reveal a structure similar to the predicted 'paired' structure. Near 39 GPa, lithium transforms to a cubic polymorph with 16 atoms per unit cell (cI16) [48], a recently discovered structure unique to lithium. Additionally, a minimum in the electronic density of states close to the Fermi energy suggests near-insulator behaviour in the paired structure.

The ambient-pressure phase of Li at low temperature is not bcc but rather a closed packed rhombohedral 9R structure. Under ambient pressure no sign of superconductivity in lithium
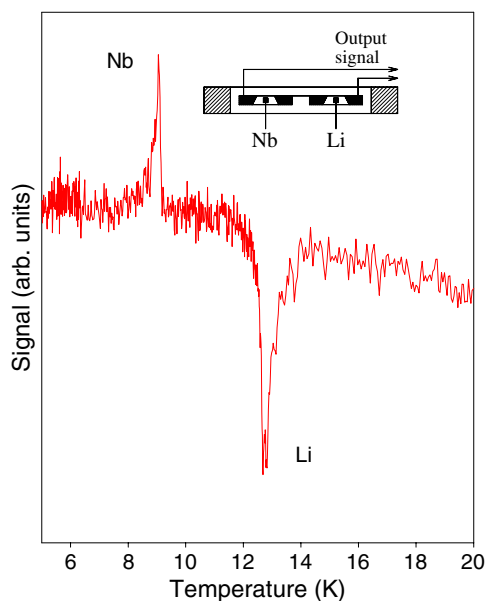
Figure 10. Magnetic susceptibility signal from a Li sample at 28 GPa. The signal from Li is superimposed on a paramagnetic background with the opposite sign. The signal from Nb in the compensating coil at ambient pressure has an inverted phase and is superimposed on the background additively.
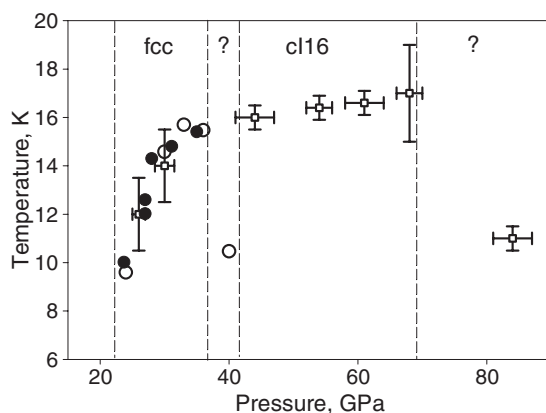
Figure 11. Pressure dependence of the T_c in lithium [43]. Open and full circles represent two susceptibility experiments; the error in pressure and T_c is less than or equal to the symbol size. The resistivity data are shown as squares. The broken lines represent possible phase boundaries.

has been detected down to 4 mK. However, it is predicted that lithium's structural changes under pressure may have significant effects on possible superconductivity in the material [49]. Explicit calculations suggest that T_c may reach a maximum of 60–80 K in the cI16 phase [49].

Because of the difficulties in studying the material under pressure (e.g. sample containment and reactivity), it is essential to apply a variety of probes to the compressed sample. For superconductivity, this includes the combination of magnetic and electrical techniques, as in our study. We find that T_c rapidly increases with pressure from 9 K at 23 GPa to 16 K at 33 GPa,

and above that pressure it drops down to 10.5 K at 40 GPa. According to our resistivity data, T_c increases to above 16 K in the range 43–46 GPa and remains almost constant to at least 60 GPa. Further increases in pressure to 80 GPa shifts the onset of the superconducting step down to 11 K. The observed changes in T_c with pressure are qualitatively compatible with the variety of phases at high pressure [49] and similar high-pressure studies [50]. However, detailed x-ray diffraction measurements at low temperatures are required to make a direct comparison with our results.

The T_c was calculated to increase dramatically in the fcc phase to 50–70 K just before the transition to hR1 (and subsequently to the cI16 phase) near 40 GPa, staying nearly constant and very high (60–80 K) in the cI16 phase from 40 to at least 80 GPa [49]. Our results are consistent with the steep increase of T_c below 30 GPa as occurred in the fcc phase, but with a much lower T_c than predicted. The drop in T_c to 10.5 K at 40 GPa may indicate that a transition to yet another phase occurs in the narrow pressure range (38–43 GPa), similar to the intermediate hexagonal phase observed by x-ray diffraction at the same pressure. Above 43 GPa, the experimental T_c values stay nearly constant at 16 K. Assuming the cI16 phase is stable in this pressure range, the theoretical prediction for the T_c is much higher than is experimentally observed. The possibility of spin fluctuations reducing T_c was discussed in the literature. The difference may also arise from the possibility of large Coulomb corrections due to electron–electron repulsion [51]. The present results add to the recent findings regarding the emerging complexity of putatively simple metals under pressure. Despite its apparent deviations from a textbook 'simple metal', however, Li remains an ideal candidate for further theoretical understanding of the origin of this complexity because of its low atomic number. While there is a possibility that the low temperature phases are distinct from those considered in [49], the discrepancies between theory and experiment may be resolved by assuming very high values of the Anderson–Morel Coulomb pseudopotential μ^* or by invoking spin fluctuation effects. The first possibility may require a full treatment of electrons and ions on the same footing similar to the approach proposed by Richardson and Ashcroft [51]. Such a treatment is likely to be very important for understanding the behaviour (including possible high temperature superconductivity) in the predicted metallic phases of hydrogen at higher pressures.

Acknowledgments

References

[1] Hemley R J and Mao H K 1997 *Encyclopedia of Applied Physics* vol 18, ed G L Trigg (New York: VCH) p 555
[2] Hemley R J and Ashcroft N W 1998 *Phys. Today* **51** 26
[3] Mao H K, Struzhkin V V, Hemley R J and Kao C C 1997 *Eos Trans. Am. Geophys. Union* **78** F774
[4] Lübbers R, Grünsteudel H F, Chumakov A I and Wortmann G 2000 *Science* **287** 1250
[5] Mao H K *et al* 2001 *Science* **292** 914
[6] Occelli F *et al* 2001 *Phys. Rev.* B **63** 224306
[7] Fiquet G, Badro J, Guyot F, Requardt H and Krisch M 2001 *Science* **291** 468
[8] Loubeyre P, LeToullec R, Hausermann D, Hanfland M, Hemley R J, Mao H K and Finger L W 1996 *Nature* **383** 702
[9] Struzhkin V V, Timofeev Yu A, Hemley R J and Mao H K 1997 *Phys. Rev. Lett.* **79** 4262

[10] Struzhkin V V, Hemley R J, Mao H K and Timofeev Y A 1997 *Nature* **390** 382

[11] Eremets M I, Shimizu K, Kobayashi T C and Amaya K 1998 *Science* **281** 1333

[12] Sturhahn W, Toellner T S, Alp E E, Zhang X W, Ando M, Yoda Y, Kikuta S, Seto M, Kimball C W and Dabrowski B 1995 *Phys. Rev. Lett.* **74** 3832

[13] Seto M, Yoda Y, Kikuta S, Zhang X W and Ando M 1995 *Phys. Rev. Lett.* **74** 3828

[14] Hu M Y, Sturhahn W, Toellner T S, Hession P M, Sutter J P and Alp E E 1999 *Nucl. Instrum. Methods Phys. Res. A* **428** 551

[15] Minkewicz V J, Shirane G and Nathans R 1967 *Phys. Rev.* **162** 528

[16] Hastings J B, Siddons D P, Bürck van U, Hollatz R and Bergmann U 1991 *Phys. Rev. Lett.* **66** 770

[17] Eng P J, Newille M, Rivers M L and Sutton S R 1998 *X-ray Microbeam Technology and Applications (Proc. SPIE.—Int. Soc. Opt. Eng.)* p 145

[18] Mao H K, Xu J and Bell P M 1986 *J. Geophys. Res.* **91** 4673

[19] Zha C S, Duffy T S, Mao H K and Hemley R J 1993 *Phys. Rev. B* **48** 9246

[20] Watt J P, Davies G F and O'Connell R J 1976 *Rev. Geophys. Space Phys.* **14** 541

[21] Watt J P and Peselnick L 1980 *J. Appl. Phys.* **51** 1525

[22] Birch F 1978 *J. Geophys. Res.* **83** 1257

[23] Fiquet G, Badro J, Guyot F, Requardt H and Krisch M 2001 *Science* **291** 468

[24] Mao H K *et al* 1998 *Nature* **396** 741

[25] Wenk H R, Matthies S, Hemley R J, Mao H K and Shu J 2000 *Nature* **405** 1044

[26] Struzhkin V V, Mao H K, Mao W, Sturhahn W, Alp E E, Shen G and Errandonea D 2004 *Hyperfine Interact.* at press

[27] Gieffers H, Lübbers R, Rupprecht K, Wortmann G, Alfè D and Chumakov A I 2002 *High Pressure Res.* **22** 501

[28] Struzhkin V V *et al* 2001 *Phys. Rev. Lett.* **87** 255501

[29] Yagi T, Suzuki T and Akimoto S 1985 *J. Geophys. Res.* **90** 8784

[30] Fei Y and Mao H K 1994 *Science* **266** 1678

[31] Mao H K, Shu J, Fei Y, Hu J and Hemley R J 1996 *Phys. Earth Planet Inter.* **96** 135

[32] Seino D 1982 *J. Magn. Magn. Mater.* **28** 55

[33] Landau L D and Lifshitz E M 1976 *Statistical Physics* part I (Moscow: Nauka)

[34] Rueff J P, Kao C C, Struzhkin V V, Badro J, Shu J, Hemley R J and Mao H K 1999 *Phys. Rev. Lett.* **82** 3284

[35] Badro J, Struzhkin V V, Shu J, Hemley R J, Mao H K, Rueff J P, Kao C C and Shen G 1999 *Phys. Rev. Lett.* **83** 4101

[36] Rueff J P *et al* 1999 *Phys. Rev. B* **60** 14510

[37] Struzhkin V V, Shen G, Badro J, Lie J, Somayazulu M, Prakapenka V, Hemley R J and Mao H K 2003 unpublished

Struzhkin V V and Eremets M I 2004 at press

[38] Gao L *et al* 1994 *Phys. Rev. B* **50** 4260

[39] Chu C W *et al* 1987 *Phys. Rev. Lett.* **58** 405

[40] Wu M K *et al* 1987 *Phys. Rev. Lett.* **58** 908

[41] Gregoryanz E, Struzhkin V V, Hemley R J, Eremets M I, Mao H K and Timofeev Yu A 2002 *Phys. Rev. B* **65** 064504

[42] Goncharov A F and Struzhkin V V 2003 *Physica C* **385** 117

[43] Struzhkin V V, Eremets M I, Gan W, Mao H K and Hemley R J 2003 *Science* **298** 1213

[44] Timofeev Yu A 1992 *Prib. Tekh. Eksp.* **5** 186 (in Russian)

[45] Timofeev Yu A, Struzhkin V V, Hemley R J, Eremets M I, Mao H K and Gregoryanz E 2002 *Rev. Sci. Instrum.* **73** 371

[46] Struzhkin V V, Timofeev Yu A, Gregoryanz E, Hemley R J and Mao H K 2002 High-pressure phenomena *Proc. Int. School of Physics* (*Enrico Fermi* vol CXLVII) ed R J Hemley, M Bernasconi, L Ulivi and G Chiarotti (Amsterdam: IOS Press/Società Italiana di Fisica) p 275

[47] Neaton J B and Ashcroft N W 2000 *Nature* **400** 141

[48] Hanfland M, Syassen K, Christensen N E and Novikov D L 2000 *Nature* **408** 174

[49] Christensen N E and Novikov D L 2001 *Phys. Rev. Lett.* **86** 1861

[50] Shimizu K *et al* 2003 *Nature* **419** 597

[51] Richardson C F and Ashcroft N W 1997 *Phys. Rev. B* **55** 15130